

Structure-Based Prediction of Subtype Selectivity of Histamine H₃ Receptor Selective Antagonists in Clinical Trials

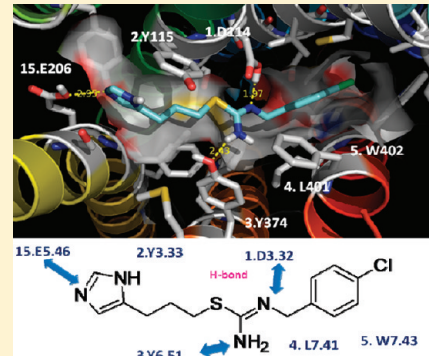
Soo-Kyung Kim,[†] Peter Fristrup,[‡] Ravinder Abrol,[†] and William A. Goddard, III^{*,†}

[†]Materials and Process Simulation Center (MC139-74), California Institute of Technology, 1200 E. California Blvd., Pasadena, California 91125, United States

[‡]Department of Chemistry, Technical University of Denmark, Kemitorvet, Building 201, 2800 Lyngby, Denmark

 Supporting Information

ABSTRACT: Histamine receptors (HRs) are excellent drug targets for the treatment of diseases, such as schizophrenia, psychosis, depression, migraine, allergies, asthma, ulcers, and hypertension. Among them, the human H₃ histamine receptor (hH₃HR) antagonists have been proposed for specific therapeutic applications, including treatment of Alzheimer's disease, attention deficit hyperactivity disorder (ADHD), epilepsy, and obesity.¹ However, many of these drug candidates cause undesired side effects through the cross-reactivity with other histamine receptor subtypes. In order to develop improved selectivity and activity for such treatments, it would be useful to have the three-dimensional structures for all four HRs. We report here the predicted structures of four HR subtypes (H₁, H₂, H₃, and H₄) using the GEnSeMBLE (GPCR ensemble of structures in membrane bilayer environment) Monte Carlo protocol,² sampling ~35 million combinations of helix packings to predict the 10 most stable packings for each of the four subtypes. Then we used these 10 best protein structures with the DarwinDock Monte Carlo protocol to sample ~50 000 × 10²⁰ poses to predict the optimum ligand–protein structures for various agonists and antagonists. We find that E206^{5,46} contributes most in binding H₃ selective agonists (**5**, **6**, **7**) in agreement with experimental mutation studies. We also find that conserved E5.46/S5.43 in both of hH₃HR and hH₄HR are involved in H₃/ H₄ subtype selectivity. In addition, we find that M378^{6,55} in hH₃HR provides additional hydrophobic interactions different from hH₄HR (the corresponding amino acid of T323^{6,55} in hH₄HR) to provide additional subtype bias. From these studies, we developed a pharmacophore model based on our predictions for known hH₃HR selective antagonists in clinical study [ABT-239 **1**, GSK-189,254 **2**, PF-3654746 **3**, and BF2.649 (tiprolisant) **4**] that suggests critical selectivity directing elements are: the basic proton interacting with D114^{3,32}, the spacer, the aromatic ring substituted with the hydrophilic or lipophilic groups interacting with lipophilic pockets in transmembranes (TMs) 3–5–6 and the aliphatic ring located in TMs 2–3–7. These 3D structures for all four HRs should help guide the rational design of novel drugs for the subtype selective antagonists and agonists with reduced side effects.



INTRODUCTION

Histamine receptors (HRs) are aminergic G protein-coupled receptors (GPCRs) with seven transmembrane (TM)-spanning helices serving as a mediator in hypersensitivity (allergic) responses, gastric acid secretion, neurotransmission, immune-modulation, cell differentiation, and embryonic development, among others.³ Four subtypes of human HRs, H₁, H₂, H₃, and H₄, have been identified.⁴ All HRs are excellent drug targets for the treatment of such diseases as schizophrenia, Alzheimer's disease (AD), dementia, anxiety, tremor (Parkinson's disease), attention deficit hyperactivity disorder (ADHD), mood disorders, sleep disorders (narcolepsy), depression, migraine, allergies, asthma, ulcers, stroke, epilepsy, obesity, diabetes, and cancer.⁵ Indeed human histamine H₁ receptor (hH₁HR) antagonists (antihistamine) are widely used in the treatment of allergy.⁶ In addition, hH₂HR antagonists are used in treating peptic ulcers, gastresophageal reflux disease, and gastrointestinal bleeding.^{7,8} The hH₃HR antagonists have been proposed for such

therapeutic applications as treatment of Alzheimer's disease, attention deficit hyperactivity disorder (ADHD), epilepsy, and obesity.¹ The hH₄HR has been suggested as an interesting drug target for the therapy of inflammation, allergy, and autoimmune disorders.⁹

While hH₁HR, hH₂HR, and hH₄HRs have been successful targets of blockbuster drugs for treating allergic diseases, gastric ulcer, and chronic constipation, the development of hH₃HR ligands still lags on their way to market, at least partly because of problems with selectivity. Thus, we decided to focus on developing an understanding of how to make ligands selective for hH₃HR.

The Results and Discussion Section describes the prediction of 3D structures for all four subtypes (H₁, H₂, H₃, and H₄) of hHRs, using the GEnSeMBLE (GPCR ensemble of structures in

Received: September 14, 2011

Published: October 29, 2011

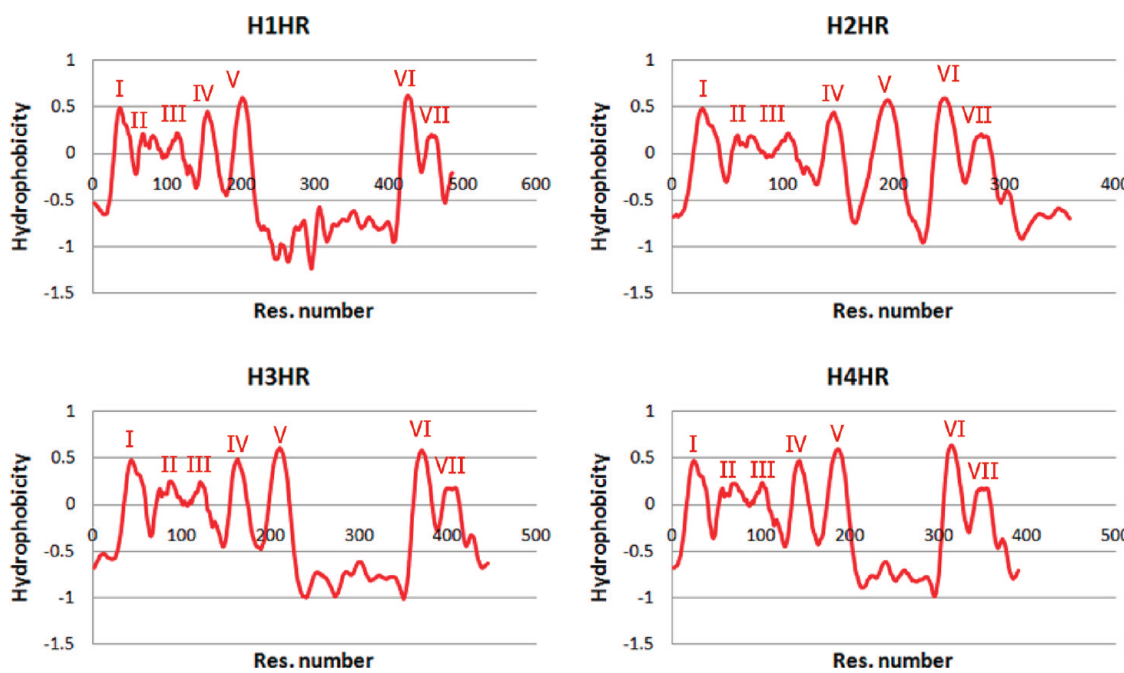


Figure 1. Hydropathy prediction from PredicTM for the four HRs.

membrane bilayer environment) method² for generating the ensemble of the 10 most stable 3D structures of these GPCRs.

Then Methods Section reports the predictions from the DarwinDock method of the binding sites for structurally known antagonists 1, 2, 3, 4 now in clinical studies, three agonists (5, 6, 7), five antagonists (clobenpropit 8 N'-[(4-chlorophenyl)methyl]-1-[3-(3H-imidazol-4-yl)propylsulfanyl]formamidine, ciproxifan 9, thioperamide 10, A-304121 [4-(3-((2R)-2-aminopropanoyl-1-piperazinyl)propoxy)phenyl]cyclopropylmethanone] 11, and A-317920 [N-((1R)-2-(4-(3-(4-(cyclopropylcarbonyl)phenoxy)-propyl)-1-piperazinyl)-1-methyl-2-oxo-ethyl)-2-furamide] 12 for the structure–activity relationship (SAR) studies.¹⁰

The Methods Section extends the comparison of the 3D structure of our predicted structure with the recently reported 3.1 Å crystal structure of the hH₁HR–T4-lysozyme fusion protein (H1R–T4L) complex with doxepin.¹¹ Since we predicted the 3D structure of all HRs when no X-ray structure of the HRs was available, this comparison will validate our methods. The 1.3 Å root mean squared deviation (RMSD) in TM between two structures reveals our atomic details of binding site, and the model will be highly useful for guiding rational design of ligands with high H₃HR selectivity.

■ RESULTS AND DISCUSSION

GENSeMBLE Predictions of Apoprotein Structures for All Four HRs. The seven TM domains of four hHRs in Figure 1 were predicted by PredicTM which combines hydrophobicity analysis and multiple sequence alignment of sequences using the MAFFT¹² program. Hydrophobic profile in the multiple sequence alignment, using the thermodynamic and biological hydrophobic scales from White and von Heijne,^{13,14} shows all hHRs have seven TM characters as shown in GPCRs; hH₂HR has a shorter intracellular three loop compared to other subtypes. Figure 2 shows the final TM regions and multiple alignments of all HRs from PredicTM. All TM regions of 4 subtypes applied by

capping rules are in good agreement within 1–5 residue difference at the terminal end.

The GENSeMBLE method² was used to predict the 3D structure of all 4 HRs before the X-ray structure of the H₁HR was reported.¹¹ In GENSeMBLE we start with some template structures and consider 12 rotations (30° pitch) about the helix axis for each of the 7 TM regions, leading to (7)¹² ~35 million packings. We then estimate the energy for all 35 million based on the pairwise interactions of the 12 strongly interacting pairs. In these calculations we start with several experimental and computational templates and finally select those with the best total interaction energies.

However when we started this project X-ray crystal structures were available for the human β₂ adrenergic receptor (PDB: 2RH1)¹⁵ and the turkey β₁ adrenergic receptor (PDB: 2VT4).¹⁶ Consequently we deviated from our standard methodology for predicting histamine receptor structures as follows:

First, the TM regions in the two templates were identified and the corresponding regions in the four histamine receptors identified based on the higher sequence homology in the TM regions (Table S1, Supporting Information). Overviews over which residues are part of the TM region for each of the four HRs are shown in Table S2, Supporting Information.

Then, each TM was mutated to match the HR of interest and energy-minimized in vacuous. Then the 7 helix bundle was used as input to the BiHelix protocol of GENSeMBLE² in which 144 combinations are considered for each pair each with reoptimized side chains. Here, each of the seven TMs was rotated systematically ±90° using a 15° sampling interval, leading to structures for the packed bundle. Then we superimposed the BiHelix energies to estimate the 1000 energetically most favored 7 TM helix bundles. These bundles were then built, the side-chains reoptimized, using the SCREAM procedure,¹⁷ and the total energies were calculated using both the standard charged model (where Asp, Glu, Lys, Arg have net charges) and the neutral model we have developed.¹⁸ From these 1000 we collected the

N-term	TM1	*	IL1			
HRH3 M E R A P P D G P L N A S G A L A G E A A A A G G A R G F S A A W T A V L A A L M A L L I V A T V L G N A L V M L A F V			60			
HRH1 - - - - - M S L P N S S C L L E D K M C E G N K T T M A S P Q L M P L V V V L S T I C L V T V G L N L L V L Y A V R			53			
HRH2 - - - - - - - - - M A P N G T A S S F C L D S T A C K I T I T V V L A V L I L I T V A G N V V V C L A V G			44			
HRH4 - - - - - - - - - M P D T N S T I N L S L S T R V T L A F F M S L V A F A I M L G N A L V I L A F V			41			
	.. . : . . : . : . : . : * : * : * .					
TM2	*	* *	*			
HRH3 A D S S L R T Q N N F F L L N L A I S D F L V G A F C I P L Y V P Y V L T G R W T F G R G L C K L W L V V D Y L L C T S	120					
HRH1 S E R K L H T V G N L Y I V S L S V A D L I V G A V V M P M N I L Y L L M S K W S L G R P L C L F W L S M D Y V A S T A	113					
HRH2 L N R R L R N L T N C F I V S L A I T D L L L G L L V L P F S A I Y Q L S C K W S F G K V F C N I Y T S L D V M L C T A	104					
HRH4 V D K N L R H R S S Y F F L N L A I S D F F V G V I S I P L Y I P H T L F E W D F G K E - I C V F W L T T D Y L L C T A	100					
: * : . : : . * : : * : : * . : * : . : * . : * : . : * : . : * : . : * : . : * : . : * : . : * : .						
IL2	TM4	*	EL2			
HRH3 S A F N I V L I S Y D R F L S V T R A V S Y R A Q Q G D T R R A V R K M L L V W V L A F L L Y G P A I L S W E Y L S G G	180					
HRH1 S I F S V F I L C I D R Y R S V Q Q P L R Y L K Y R T K T - R A S A T I L G A W F L S F L W V I P I / L G W N H F M Q Q T	172					
HRH2 S I L N L F M I S L D R Y C A V M D P L R Y P V L V T P V - R V A I S L V L I W V I S I T L S F L S I H L G W N S R N E T	164					
HRH4 S V Y N I V L I S Y D R Y L S V S N A V S Y R T Q H T G V L K I V T L M V A V W V L A F L V N G P M I L V S E S W K D E	160					
* . : . : : . * * : : * . : * . : * . : * . : * . : * . : * . : * . : * . : * . : * . : * . : * . : * .						
TM5	*	* *	IL3			
HRH3 S S I P E G H C Y A E F F Y N W Y F L I T A S T L E F F T P F L S V T F F N L S I Y L N I Q R R T R L R L D G A R E A A	240					
HRH1 S V R R E D K C E T D F Y D V T W F K V M T A I I N F Y L P T L L M L W F Y A K I Y K A V R Q H C Q H R E L I N R S L P	232					
HRH2 S K G N H T T S K C K V Q V N E V Y G L V D G L V T F Y L P L L I M C I T Y Y R I F K V A R D Q A K R - - - - - - - - -	215					
HRH4 G S E - - - C E P G F F S E W Y I L A I T S F L E F V I P V I L V A Y F N M N I Y W S L W K R D H L - - - - - - - - -	207					
. : * * : * : * : . : * : * : . : * : * : . : * : . : * : . : * : . : * : . : * : . : * : . : * : . : * : .						
TM6	*	EL3	TM7	*	* *	*
HRH3 V A K S L A V I V S I F G L C W A P Y T L L M I I R A A C H G H C V P - D Y W Y E T S F W L L W A N S A V N P V L Y P L	414					
HRH1 A A K Q L G F I M A A F I L C W I P Y F I F F M V I A F C K N C N E - - H L H M F T / I W L G Y I N S T L N P L I Y P L	470					
HRH2 A T V T L A A V M G A F I I C W F P Y F T A F V Y R G L R G D D A I N - E V L E A I V L W L G Y A N S A L N P I L Y A A	290					
HRH4 L A K S L A I L L G V F A V C W A P Y S L F T I V L S F Y S S A T G P K S V W Y R I A F W L Q W F N S F V N P L L Y P L	360					
: * . : : . * : * * : * * : . : . : . : . : * * : * * : * * : * * : * .						
IL4	TM8	*	EL4	*	* *	*
HRH3 C H H S F R R A F T K L L C P Q K L K I Q P H S S L E H C W K -	445					
HRH1 C N E N F K K T F K R I L H I R S -	487					
HRH2 L N R D F R T G Y Q Q L F C C R L A N R N S H K T S I R S N A S Q L S R T Q S R E P R Q Q E E K P L K L Q V W S G T E V	350					
HRH4 C H K R F Q K A F L K I F C I K K Q P L P S Q H S R S V S S -	390					
: * : . : : . * : : : : .						

Figure 2. Alignments of the four HR subtypes, H₁, H₂, H₃, and H₄ from the PredicTM method. The predicted TM regions from PredicTM are displayed in colored boxes (TM1 in purple, TM2 in blue, TM3 in cyan, TM4 in green, TM5 in yellow, TM6 in orange, TM7 in red). Highly conserved residues in family A GPCRs are shown in red in TM1–6 and white in TM7. Variable amino acids among the four subtypes in the upper TM regions are marked with red asterisks, and subtype selective residues predicted from the cavity analysis are boxed. We use Ballesteros–Weinstein numbering consisting of the TM helix number followed by residue number relative to the highly conserved residue in the helix, numbered as 50. H-bonding is indicated by arrows, and subtype selective residues are shown in red.

best 10 in Table 1 for each combination of HR and template. These results make it clear that for hH₁HR and hH₃HR the structures derived from the human β_2 adrenergic receptor were significantly more favorable energetically than models derived from the turkey β_1 adrenergic receptor. In contrast, for hH₂HR and hH₄HR the structures derived from the turkey β_1 adrenergic receptor were most favorable.

For these best 10 structures, we examine new configurations including rotations of $\pm 15^\circ$ for TM3, -15° , $\pm 30^\circ$, 45° for TM4, and 15° for TMS. We found that the structure derived directly from the initial helix bundle (i.e., with $\eta = 0^\circ$ for all 7 helices) was not unreasonably high in energy. This preference for structures near 0° supports the applicability of these two X-ray crystal structures as a reasonable starting point for the BiHelix sampling. Indeed, the top-scoring structures for all four HRs differed in the rotation of only a single *one* of the seven TMs. For hH₃HR, the top-scoring model had a -30° rotation of TM4 (human β_2 adrenergic receptor as template), whereas for hH₁HR the top-scoring model had a $+15^\circ$ rotation of TM4 (human β_2 adrenergic receptor as template). Moreover for hH₂HR the top-scoring model had a -15° rotation of TM4 (turkey β_1 adrenergic receptor as template), while for hH₄HR the top-scoring model

had a +15° rotation of TMS (turkey β_1 adrenergic receptor as template).

Compared with hH₁HR (20.90% in overall, 32.15% in TM) and hH₂HR (17.30% in overall, 33.08 in TM) with low sequence identity in Table S1 in Supporting Information, hH₄HR has a sequence identity of 34.83% to hH₃HR and 54.84% in TM regions. Many compounds with reported affinity for hH₃HR also have affinity for hH₄HR. Compounds like clozapine and cloben- propit behave as partial agonists at hH₄HR and as antagonists at hH₃HR, showing some functional selectivity.¹⁹ Many drug candidates cause undesired side effects through their cross-reactivity. To develop improved selectivity and activity for such treatments, we use the 10 most stable three-dimensional structures for all four HRs.

Predicted Structures for Ligands Binding to All Four HRs.

First generation hH₃HR antagonists were monoalkyl-substituted imidazole-based derivatives like thioperamide, clobenpropit, or ciproxifan.²⁰ Potent stimulation of hH₃HR has been observed by imidazole derivatives only. Claimed interaction potential to cytochrome P450 (CYP) isozymes caused by the imidazole moiety related to elements of the porphyrine cycle and sometimes complex pharmacological behavior led to imidazole-

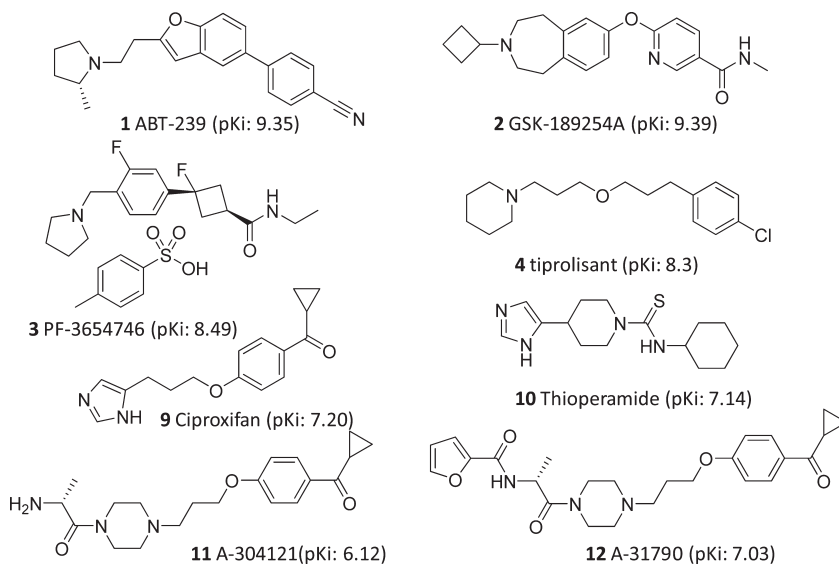
Table 1. Top 10 Predicted Structures of the 4 hHRs from the CombiHelix Analysis of the $(13)^7 = 62\,748\,517$ BiHelix Packing Geometries Within $\pm 90^\circ$ Angle Range by 15° Increments^a

hH ₃ HR- β 2*											
#	H1	H2	H3	H4	H5	H6	H7	CIH	CTot	NIH	NTot
H1-1	0	0	0	15	0	0	0	-229.2	803.0	-387.6	354.2
H1-2	0	0	0	0	0	0	0	-207.4	816.7	-374.6	358.0
H1-3	0	0	0	-15	0	0	0	-245.1	814.0	-388.8	376.4
H1-4	0	0	0	0	0	0	90	-171.0	861.0	-360.8	387.9
H1-5	0	0	0	0	0	-15	0	-168.6	852.6	-344.5	395.1
H1-6	0	-15	0	0	0	0	0	-204.8	847.9	-365.0	395.9
H1-7	-15	0	0	15	0	0	0	-217.5	852.7	-380.5	395.9
H1-8	90	0	0	0	0	0	0	-183.4	849.1	-341.9	399.1
H1-9	-15	0	0	0	0	0	0	-190.2	840.2	-358.7	401.3
H1-10	0	0	0	30	0	0	0	-200.6	846.5	-365.3	401.8

hH ₃ HR- β 1*											
#	H1	H2	H3	H4	H5	H6	H7	CIH	CTot	NIH	NTot
H2-1	0	0	0	-15	0	0	0	-502.8	51.0	-390.7	33.9
H2-2	-75	0	0	-15	0	0	90	-462.7	78.9	-354.6	56.0
H2-3	0	0	0	-15	0	0	90	-466.6	106.7	-372.9	64.6
H2-4	-90	0	0	-15	0	0	-15	-478.8	77.6	-361.0	65.8
H2-5	-90	0	0	-15	0	0	90	-446.5	99.7	-348.0	66.8
H2-6	0	0	0	0	0	0	0	-487.9	98.6	-380.4	67.2
H2-7	-90	0	0	-15	0	45	-30	-470.4	94.4	-351.1	71.0
H2-8	-15	0	0	-15	0	0	0	-482.4	92.9	-366.4	78.0
H2-9	0	0	0	-15	-15	0	0	-479.4	91.1	-374.5	78.7
H2-10	-15	0	0	-15	0	0	90	-441.1	130.8	-345.5	85.9

^a All 1000 models from CombiHelix were selected for neutralization by their charge total energy (*E*) score (ChargeTot: kcal/mol). The final 100 models were ordered by neutral total *E* (NeutTot: kcal/mol). The case with $\eta = 0^\circ$ for all 7 helices is represented in italic, and the best *E* is shown in bold. CIH is charge interhelical energy, CTot is charge total energy, NIH is neutral interhelical energy, and NTot is neutral total energy. *The case with $\eta = 0^\circ$ for all 7 helices is ranked as 12 (*E*: 43.6 kcal/mol) in hH₃HR- β 2 and 34 in hH₄HR- β 1 (*E*: 298.9 kcal/mol), respectively.

Chart 1. Chemical Structures of Structurally Known Histamine H₃ Receptor Antagonists in Clinical Study, ABT-239 1, GSK-189254A 2, PF-3654746 3, and BF2.649 (Tiprolisant) 4^a



^a Binding affinities (pK_i) are shown for H₃ with its function in parentheses compared to the endogenous histamine.

replacements. A general pharmacophore element of these nonimidazole derivatives has been described which is nowadays shown in numerous variations and combinations: A basic moiety is linked

by a spacer to a central, mostly aromatic core structure which then is connected to further affinity enhancing elements, e.g., another basic moiety or hydrophilic/lipophilic groups or a combination thereof.²¹

Table 2. Cavity Energy of the Endogenous Agonist Histamine Bound to the Human Histamine H₃ Receptor (hH₃HR)^a

Res. #	vdW	Coulomb	H-Bond	NonBond	Mutation	Ki (nM)
E206	1.69	-2.80	-3.97	-5.08	E206A	32550.00
F207	-4.00	0.18	0.00	-3.81		
Y115	-2.91	-0.17	0.00	-3.09		
D114	4.42	-1.89	-4.66	-2.12		
C118	1.00	-0.17	-1.47	-0.64		
Y374	-0.48	-0.12	0.00	-0.60		
T119	-0.66	0.17	0.00	-0.49		
Y167	-0.45	-0.03	0.00	-0.47		
L401	-0.48	0.05	0.00	-0.43		
F398	-0.28	-0.06	0.00	-0.33		
T204	-0.29	0.00	0.00	-0.30	T204A	91.00
W371	-0.22	-0.06	0.00	-0.28		
M378	-0.25	-0.03	0.00	-0.28		
S203	-0.31	0.13	0.00	-0.18		
F211	-0.15	-0.01	0.00	-0.16		
L111	-0.13	0.03	0.00	-0.10		
W174	-0.07	-0.01	0.00	-0.08		
I171	-0.04	-0.03	0.00	-0.07		
W402	-0.02	0.00	0.00	-0.02		
A202	-0.09	0.10	0.00	0.01	A202Q	66.68
SUM				-18.52	WT	15.86

^a Residues are ordered by total NonBond energy, which is the sum of van der Waals (vdW), Coulomb, and H-bond energy (kcal/mol) in the unified cavity. The color coding for contributions of each residue to binding of the adenosine ligand is: dark grey: > 3 kcal/mol, grey: 1 - 3 kcal/mol, light grey: 0.5 - 1.0 kcal/mol. The experimental point-mutation result was compared.

A number of hH₃HR antagonists have advanced to the clinical area for the potential treatment of human cognitive disorders.²² These include 4-(2-{[2R]-2-methylpyrrolidin-1-yl}ethyl)-benzofuran-5-yl)benzonitrile, (ABT-239 1), 6-[{(3-cyclobutyl-2,3,4,5-tetrahydro-1H-3-benzazepin-7-yl)oxy]-N-methyl-3-pyridinecarboxamide hydrochloride (GSK189254 2), (1R,3R)-N-ethyl-3-fluoro-3-[3-fluoro-4-(pyrrolidin-1-ylmethyl)phenyl]cyclobutane-1-carboxamide (PF-03654746 3), 1-{3-[3-(4-chlorophenyl)propoxy]propyl} piperidine hydrochloride (BF2.649 4), MK-0249 (structure not yet disclosed), JNJ-17216498 (structure not yet disclosed), and ABT-288 (structure not yet disclosed).

Among these, we selected structurally known compounds (structures shown in Chart 1) like ABT-239 1 (pK_i : 9.35 at hH₃HR), for cognitive disorder (Phase I),²³ GSK-189254A 2 (pK_i : 9.59 at hH₃HR) for dementia, narcolepsy, and schizophrenia (Phase I),²⁴ PF-3654746 3 (pK_i : 8.49 at hH₃HR) for allergic rhinitis (Phase II), and BF2.649 4 (tiprolisant, pK_i : 8.3 at hH₃HR) for central nervous system disease: hypersomnina and narcolepsy (Phase II)²⁵ for docking studies.

As summarized in the Methods Section, the DarwinDock method for predicting ligand binding sites starts by sampling the full protein to locate putative binding regions and then aims at sampling a complete set of ligand conformation (~20) for each; of which we sample a complete set of poses (~50 000) from which we select the best poses using the total binding energy, E .

Endogenous Agonist Histamine. We docked histamine, the endogenous agonist 5, to the lowest E predicted structure of hH₃HR in Table 1 from CombiHelix.

Most of poses show salt bridges at D114^{3,32} or E206^{5,46} with the protonated nitrogen atom or one of the nitrogen atoms in

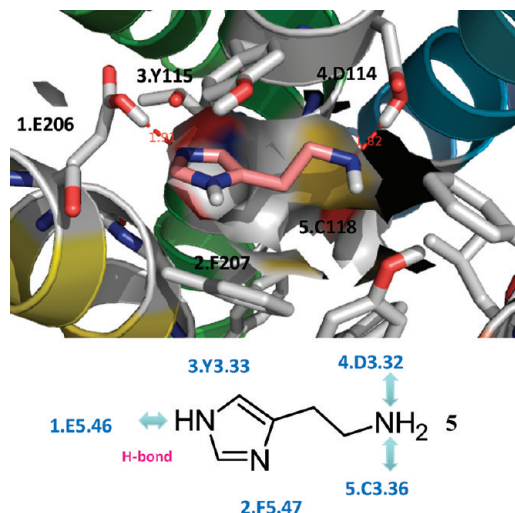


Figure 3. Predicted best models of the endogenous agonist histamine 5 bound to hH₃HR. The H-bonding is represented by the arrows with the distance between the donor and the acceptor. The number with residue is from the order of unified cavity E in Table 2. Schematic structure of the predicted binding sites is displayed in the bottom figure.

the imidazole ring. Our cavity analysis (Table 2) of the histamine bound to hH₃HR shows that the major contributing amino acids in ligand binding are E206^{5,46} (-5.08 kcal/mol), F207^{5,47} (-3.81 kcal/mol), Y115^{3,33} (-3.09 kcal/mol), and D114^{3,32} (-2.12 kcal/mol) based on nonbonding energies (defined in the Methods Section as the sum of vdW, electrostatic Coulomb with 2.5 dielectric constant, and H-bond energies). This result agrees with previous docking studies which shows all hydrophilic interactions at D114^{3,32}/E206^{5,46} and hydrophobic interactions at Y115^{3,33}, Y374^{6,51}, and F398^{7,39}, as found in bovine rhodopsin-based hH₃HR homology models.²⁶ Histamine has similar interactions in hH₄HR with the main interaction at D114^{3,32}/E206^{5,46}.^{27,28} Supporting this, the Ala mutation of E206^{5,46}, which was the most major contributing residue in the cavity analysis (Table 2), shows dramatic loss of agonist with more than 2000-fold decrease. In addition, T204A^{5,44} and A202Q^{5,42} mutants display substantial decrease of histamine binding with 5.7- and 4.2-fold decrease compared with the wild-type, respectively.²⁶

In the neutral system of histamine-hH₃HR, we find that the deprotonated nitrogen atom of the histamine interacts with the protonated D114^{3,32}, while the protonated E206^{5,46} also H-bonds with the ε-NH atom in the imidazole ring of histamine, as shown in Figure 3. An additional hydrophobic interaction occurs at F207^{5,47} and Y115^{3,33}.

hH₃HR Selective Agonists 5, 6, 7. We next matched the H₃ selective agonist, (R)-α-methyl histamine 6, to validate the binding site of histamine at hH₃HR, leading to common interactions at E206^{5,46} (-4.73 kcal/mol), F207^{5,47} (-3.99 kcal/mol), D114^{3,32} (-2.96 kcal/mol), and Y115^{3,33} (-2.38 kcal/mol). However, the stereoisomer, (S)-α-methyl histamine 7, with ~100-fold less binding affinity reveals unfavorable interactions at Y115^{3,33} (+6.84 kcal/mol) because of the bad contact with the α-methyl group (Table 3 and Figure 4). The result is a dramatic decrease in binding affinity (cavity sum = -18.07 for (R)-α-methyl histamine 6 vs -8.39 for (S)-α-methyl histamine 7) in agreement with the dramatically decreased experimental binding affinity of (S)-α-methyl

Table 3. Cavity Energy of the H₃ Selective Agonist (*R*)- α -Methyl Histamine vs (*S*)- α -Methyl Histamine at hH₃HR^a

Res. #	(<i>R</i>)- α -methyl histamine (Pki: 8.2)				(<i>S</i>)- α -methyl histamine (Pki: 7.2)			
	VdW	Coulomb	H-Bond	NonBond	VdW	Coulomb	H-Bond	NonBond
E206	2.50	-2.91	-4.31	-4.73	1.41	-2.82	-4.00	-5.41
F207	-4.15	0.16	0.00	-3.99	-3.54	0.06	0.00	-3.49
D114	3.48	-1.89	-4.55	-2.96	2.17	-1.19	-3.67	-2.69
<i>Y115</i>	-2.13	-0.25	0.00	-2.38	6.97	-0.13	0.00	6.84
Y374	-0.66	-0.15	0.00	-0.81	-0.69	-0.16	0.00	-0.85
T119	-0.70	0.15	0.00	-0.56	-0.66	0.19	0.00	-0.47
Y167	-0.50	-0.02	0.00	-0.52	-0.49	-0.04	0.00	-0.53
F398	-0.48	-0.04	0.00	-0.52	-0.38	-0.06	0.00	-0.44
L401	-0.48	0.05	0.00	-0.43	-0.13	0.05	0.00	-0.08
M378	-0.29	-0.03	0.00	-0.32	-0.30	-0.03	0.00	-0.32
W371	-0.26	-0.06	0.00	-0.31	-0.29	-0.06	0.00	-0.35
T204	-0.30	0.01	0.00	-0.30	-0.31	0.02	0.00	-0.29
S203	-0.45	0.18	0.00	-0.28	-0.57	0.28	0.00	-0.29
F211	-0.17	-0.02	0.00	-0.18	-0.18	-0.02	0.00	-0.20
L111	-0.20	0.05	0.00	-0.15	-0.20	0.00	0.00	-0.20
L117	-0.16	0.05	0.00	-0.12	-0.20	0.06	0.00	-0.14
W174	-0.09	0.00	0.00	-0.10	-0.08	0.00	0.00	-0.09
I171	-0.05	-0.03	0.00	-0.08	-0.05	-0.03	0.00	-0.07
V83	-0.09	0.01	0.00	-0.08	-0.10	0.01	0.00	-0.09
C118	3.53	-0.22	-2.58	0.73	2.28	-0.14	-1.41	0.73
SUM				-18.07				-8.39

^a Residues are ordered by total NonBond energy of (*R*)-methyl histamine, which is the sum of vdW, Coulomb, and H-bond energy (kcal/mol) in the unified cavity. (*S*)- α -methyl histamine with \sim 100-fold less binding affinity²⁹ displayed unfavorable interaction at Y115 with α -methyl groups in italic font. The color coding for contributions of each residue to binding of the adenosine ligand is: dark grey: > 3 kcal/mol, grey: 1–3 kcal/mol, light grey: 0.5–1.0 kcal/mol.

histamine 7 at hH₃HR (pK_i at hH₃HR: 8.2 for **6** vs 7.2 for **7**).²⁹

The cavity analysis of the H₃ selective agonists (**5**, **6**, **7**) suggests the major contributing amino acid is E206^{5,46} (Tables 2 and 3). These docking results are in good agreement with the current mutational study. The most pronounced reduction in potency and affinity of the agonists was seen with the mutation of E206^{5,46,26}.

Thus the stereoselectivity of the methylated histamine derivatives is explained by these docking studies. The result agrees with experimental observations that the methylated histamine derivative, (*R*)- α -methylhistamine, is the more selective and the potent hH₃HR agonist. The (*S*)-stereoisomer is about 100 times less potent than the (*R*)-isomer.²⁹

Docking of hH₃HR Selective Antagonist **8, Clobenpropit, at All Four HRs and Further SAR Studies.** Antagonist docking started from the assumption that classical H₃ antagonists, such as monoalkyl-substituted imidazole-based derivatives, would share the interaction between their imidazole ring and E206^{5,46}, as shown in the endogenous agonist, histamine **5**. This hypothesis is based on the partial structural similarity between histamine and imidazole-containing H₃ antagonists (i.e., the imidazole ring, the spacer, and the basic or polar portion).

We docked hH₃HR selective antagonist **8**, clobenpropit, to the lowest *E* predicted structures of all four hHRs of Table 1. From the cavity analysis of H₃ subtype selective clobenpropit **8** bound to hH₃HR, Table 4 shows that the major contributing amino acids are Y115^{3,33} (−4.96 kcal/mol), W402^{7,43} (−4.71 kcal/mol), and D114^{3,32} (−3.73 kcal/mol). The major H-bonding is shown at D114^{3,32} and Y374^{6,51} with the isothiourea group. Additional H-bonding with the terminal imidazole ring is formed

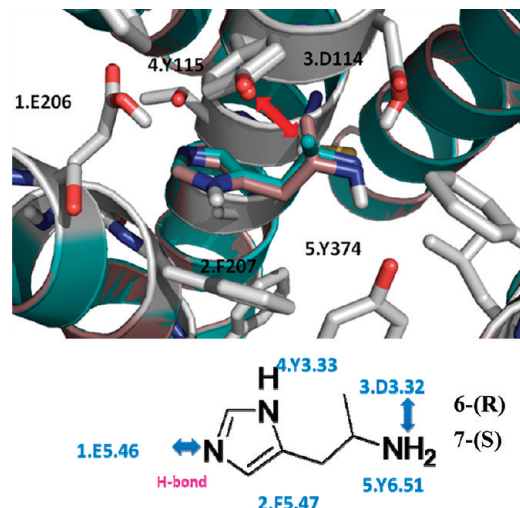


Figure 4. Superposition of the H₃ selective agonist (*R*)- α -methyl histamine **6** and (*S*)- α -methyl histamine **7** to the hH₃HR. The H-bonding is represented by the arrows between the donor and the acceptor. (*S*)- α -methyl histamine with \sim 100-fold less binding affinity displayed unfavorable interaction at Y115 with α -methyl groups in red arrow. The number with residue is from the order of unified cavity E in Table 3. Schematic structure of the predicted binding sites is displayed in the bottom figure.

at E206^{5,46}. The para-chloro-benzyl group of clobenpropit **8** is surrounded by hydrophobic residues, L401^{7,42} and W402^{7,43}, as shown in Figure 5.

Table 4. Cavity Energy of the H₃ Selective Antagonist Clobenpropit 8 to Four Human HRs^a

Ballesteros-Weinstein #	hH ₃ HR (pKi: 9.4)		hH ₄ HR (pKi: 7.4)		hH ₁ HR (pKi: 5.6)		hH ₂ HR (pKi: 5.2)	
	Res. #	NonBond						
3.33	Y115	-4.96	Y95	-5.70	Y108	-5.41	V99	-3.45
7.43	W402	-4.71	W348	-5.20	Y458	-4.02	Y278	-2.78
3.32	D114	-3.73	D94	-3.55	D107	-2.73	D98	-5.19
6.51	Y374	-2.54	Y319	-2.51	Y431	-3.65	Y250	-3.19
5.43	S203	-2.43	S179	-1.79	A195	-0.53	G187	-1.21
5.46	E206	-2.22	E182	-3.39	N198	-1.92	T190	-1.07
3.28	W110	-1.68	W90	0.00	W103	-1.60	Y94	0.00
3.36	C118	-1.66	C98	-3.11	S111	-3.63	C102	-2.80
2.57	C87	-1.58	S68	-2.02	V80	-1.47	V71	-2.24
2.53	V83	-1.33	V64	-1.26	V76	2.25	L67	0.15
6.55	M378	-1.28	T323	-0.41	F435	-1.66	F254	-2.40
2.51	Y81	-1.27	Y72	-1.35	N84	-0.84	S75	-0.67
7.39	F398	-1.20	F344	-0.12	I454	-1.12	L274	-0.98
6.48	W371	-1.14	W316	-0.58	W428	-1.51	W247	-2.83
2.58	I88	-1.03	I69	-0.78	M81	0.14	L72	-1.25
5.47	F207	-0.77	F183	-1.07	F199	-0.48	F191	-0.83
3.35	L117	-0.75	L97	-0.95	A110	-0.65	L101	-0.73
3.37	T119	-0.74	T99	-0.50	T112	-0.74	T103	-0.39
6.52	T375	-0.60	S320	-0.24	F432	-1.06	F251	-0.81
5.39	L199	-0.57	L175	-0.45	K191	-0.22	G183	-0.22
5.42	L401	-0.39	Q347	0.03	G457	-0.22	G457	0.00
3.31	V113	-0.34	T93	-0.43	M106	-0.41	L97	0.00
5.38	F198	-0.15	I174	-0.14	F190	0.00	Y182	0.00
4.57	Y167	0.00	N147	0.15	V159	-0.64	S150	0.00
4.61	I171	0.00	I151	0.00	L163	-0.31	I154	0.00
7.40	W399	0.00	W345	0.00	W455	0.00	W275	-0.75
7.46	S405	0.00	S351	0.00	S461	-0.23	S281	0.00
5.42	A202	0.13	T178	0.23	T194	-1.47	D186	-0.13
	SUM	-36.94	SUM	-35.12	SUM	-34.11	SUM	-33.77

^a Residues are ordered by total NonBond energy (H₃), which is the sum of vdW, Coulomb, and H-bond energy (kcal/mol) in the unified cavity. Predicted subtype residues that vary among four subtypes (H₄: 29%, 8/28, H₁: 57%, 16/28, H₂: 68%, 19/28) are displayed in italic font. The color coding for contributions of each residue to binding of the adenosine ligand is: dark grey: > 3 kcal/mol, grey: 1 - 3 kcal/mol, light grey: 0.5 - 1.0 kcal/mol. In the Ballesteros-Weinstein numbering, the most conserved residue in each of the seven TM domains is taken as the reference and numbered as 50. This residue is designated x.50 where x is the number of the TM helix.

To understand subtype selectivity, we matched the predicted best binding pose of the highly H₃-selective ligand clobenpropit 8 at hH₃HR to other three subtypes (H₁, H₂, H₄) of hHRs, and then we used SCREAM¹⁷ to predict the optimum side chain position of residues in the binding pocket, after which we minimized the final ligand/protein complex post neutralization. Predicted subtype residues that vary among four subtypes (H₄: 29%, 8/28, H₁: 57%, 16/28, H₂: 68%, 19/28) are displayed in Table 4. The corresponding amino acids of conserved E5.46/S5.43 in both of hH₃HR and hH₄HR are N198^{5,46}/A195^{5,43} in hH₁HR and T190^{5,46}/G187^{5,43} (Figure 2). Both of two subtype variable residues in hH₁HR and hH₂HR show weakened interactions in the cavity in Table 4 and Figure 6, resulting in a 2.2–2.4 kcal/mol favorable interaction in hH₃HR. However, the similar interaction is shown at these two conserved residues of hH₄HR. Thus, the final cavity sum is a substantial decrease in binding affinity (cavity sum = -34.11 in hH₁HR, -33.77 in hH₂HR) in agreement with the dramatically decreased experimental binding affinity at hH₁HR (pK_i: 5.6) and hH₂HR (pK_i: 5.2). The final cavity sum with the weakened binding affinity at hH₄HR (pK_i: 7.4) is a -35.12 kcal/mol compared with the

cavity sum of hH₃HR (pK_i: 9.4), -36.94 kcal/mol. Thus, this predicted binding energy is consistent with the experimental binding affinity of H₃ subtype selective clobenpropit 8.³⁰ The predicted structures were ordered by experimental binding affinity, including unified cavity energy (UniCav E) in Table 5 in all subtypes of hHRs. Furthermore, all scoring energies at all HRs parallel with their experimental binding affinities with the *r*² values (correlation coefficients) of 0.67 to 0.99 (Figure 7).

For further SAR studies, we included four more antagonists, ciproxifan 9, thioperamide 10, A-304121 11, and A-317920 12 in the same literature.³⁰ Predicted binding cavity energies for eight models in good agreement with experimental relative binding constants (*r*² = 0.65 for all 8 and *r*² = 0.93 for 6 excluding the flexible ligands, A-304121 11, and A-317920 12, which include more than 10 rotatable bonds in their structures in Figure 7). All of them share the same binding site with major anchoring site at D114^{3,32} in Figure 6.

Based on the docking studies of the subtype selective antagonist clobenpropit 8, we suggest that E5.46/S5.43 in hH₃HR and hH₄HR are involved in additional H-bonding

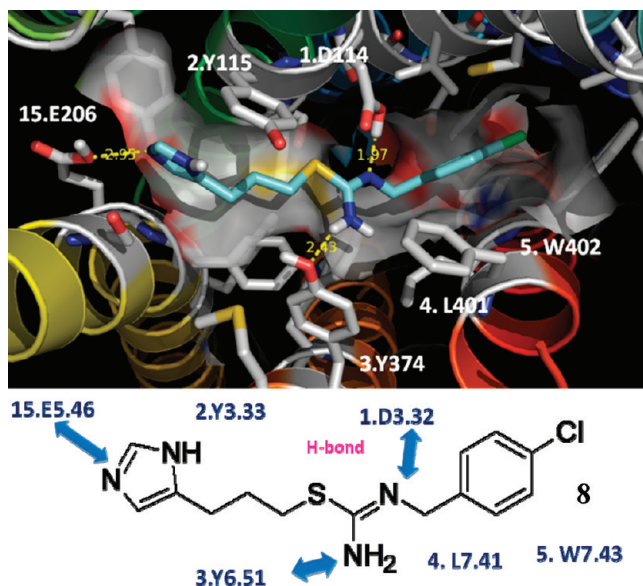


Figure 5. Predicted best models of the H_3 selective antagonist clobenpropit 8 bound to the hH_3HR . The H-bonding is represented by the arrows between the donor and the acceptor. The number with residue is from the order of unified cavity E in Table 5. Schematic structure of the predicted binding sites is displayed in the bottom figure.

interactions with the terminal imidazole group in the mono-alkyl-substituted imidazole-based derivatives, however these interactions are lost in hH_1HR and hH_2HR , as shown in Figure 6. Supporting this, sequence alignments show that TMs of the hHRs is poorly conserved, suggesting a potential differences in the mechanism in which histamine binds to the hH_3HR . For the difference between hH_3HR and hH_4HR , M378^{6,55} in hH_3HR (which is the corresponding amino acid of T323^{6,55} in hH_4HR) stabilizes through additional hydrophobic interactions (-1.28 kcal/mol at M378^{6,55} vs -0.41 kcal/mol at T323^{6,55}). Thus this predicted structure explains the increase of H_3 selectivity for clobenpropit 8 at hH_3HR over the other three subtypes.

In addition, scoring energy of hH_3HR selective antagonist clobenpropit for all HRs correlates with the observed experimental binding affinities with r^2 values (correlation coefficients) of 0.69–0.98.

Docking of Structurally Known hH_3HR Selective Antagonists in Clinical Studies. Docking studies were also carried out using structurally known hH_3HR selective antagonists in clinical trials, ABT-239 1, GSK-189,254 2, PF-3654746 3, and BF2.649 4. To develop a general pharmacophore model for these nonimidazole derivatives with hH_3HR selectivity, we selected structurally known hH_3HR targeting drugs in phase I or II preclinical studies, ABT-239 1 (pK_i : 9.35), GSK-189254A 2 (pK_i : 9.59), PF-3654746 3 (pK_i : 8.49), and BF2.649 4 (tiprolisant, pK_i : 8.3) for further docking studies.

As shown in Figure 8, the binding sites of four antagonists overlap, as expected. A central basic moiety shows common H-bonding at D114^{3,32}. An aromatic core structure leads to further affinity enhancing elements, e.g., hydrophilic/lipophilic groups are surrounded by hydrophobic cavity in TMs 3–5–6 region. The aliphatic ring including a protonated nitrogen is surrounded by another hydrophobic cavity in TMs 2–3–7.

Table 5. Calculated Binding Energies (E , kcal/mol) of the H_3 Selective Antagonist Clobenpropit 8 Bound to Four Human HR and Other Antagonists (Ciproxifan 9, Thioperamide 10, A-304121 11, A-317920 12 at hH_3HR ^a

Compound/hHRs	pKi	LocalCav	UnifiedCav	Snapbe	SnapbeSolv
Clobenpropit/ hH_3HR	9.44	-36.94	-38.29	-61.09	-48.85
Clobenpropit/ hH_4HR	7.38	-35.12	-36.07	-56.62	-45.06
Ciproxifan/ hH_3HR	7.20	-34.58	-35.85	-42.48	-30.18
Thioperamide/ hH_3HR	7.14	-34.79	-36.93	-45.33	-32.32
A-317920/ hH_3HR	7.03	-33.40	-36.88	-59.12	-41.60
A-304121/ hH_3HR	6.12	-34.81	-37.41	-69.14	-53.57
Clobenpropit/ hH_1HR	5.56	-34.11	-35.01	-55.29	-44.33
Clobenpropit/ hH_2HR	5.24	-33.77	-34.30	-48.46	-36.20

^a Energetically favorable E is in grey shading. LocalCav: local cavity E , UnifiedCav: unified cavity E , Snapbe: snap binding E = complex E – (protein E – ligand E), SnapbeSolv: snap binding E including solvation E with Delphi method

GSK-189254A 2 shows an extra H-bond at S203^{5,43} with the nitrogen atom in the pyridine ring. PF-3654746 3 also forms additional H-bonding interactions among the terminal amino group, Y194^{5,34} and E206^{5,46}, and between F substituent and Y374^{6,51}.

All hH_3HR selective antagonists could be mutually superposed following a common pharmacophore model with similar arrangements at the same binding site. The proposed pharmacophore model suggests the basic proton interacting with D114^{3,32}, the spacer, the aromatic ring substituted with the hydrophilic or lipophilic groups interacting with lipophilic pockets in TMs 3–5–6 and the aliphatic ring located in TMs 2–3–7. This model is in good agreement with the current generally accepted model; a basic amine motif separated by several atoms from the central, typically hydrophobic, core, which is joined on the other side by a structurally variable region in the form of another basic amine or a polar, nonbasic arrangement (e.g., amide).⁵

Structure Comparison of Predicted Structure and the Experimental X-ray Structure of the hH_1HR (PDB ID: 3RZE).

¹¹ Compared to the crystal structure of the hH_1HR , the RMSD of the predicted hH_1HR structure generated by our GEnSeMBLE method showed 1.33 Å RMSD in whole TMs, as shown in Table 6. There were also no big differences with other subtypes in the average backbone RMSD of TM helices with less than 1.64 Å for all three hH_2HR (1.64 Å), hH_3HR (1.33 Å), and hH_4HR (1.60 Å). The most similar structure of hH_1HR is hH_3HR with 0.04 Å. Among TMs major structural deviations are shown at the TMs 1 and 5 with 0.85 and 0.84 Å RMSD, respectively.

The recent availability of GPCR crystal structures provides some mechanistic insights into both the inactive and active forms, which should be useful in designing ligands for therapeutic applications. These results show that the seven-helix TM topology of these receptors can exhibit multiple conformations with variations in interhelical orientations, which in turn can change the binding site and energy of various ligands. These multiple conformations are observed both for a given GPCR in different functional forms (e.g., inactive vs active) and across different GPCRs. The conformational variations already found in the crystallized GPCRs strongly suggest that homology models based on a single template would not be sufficiently flexible to

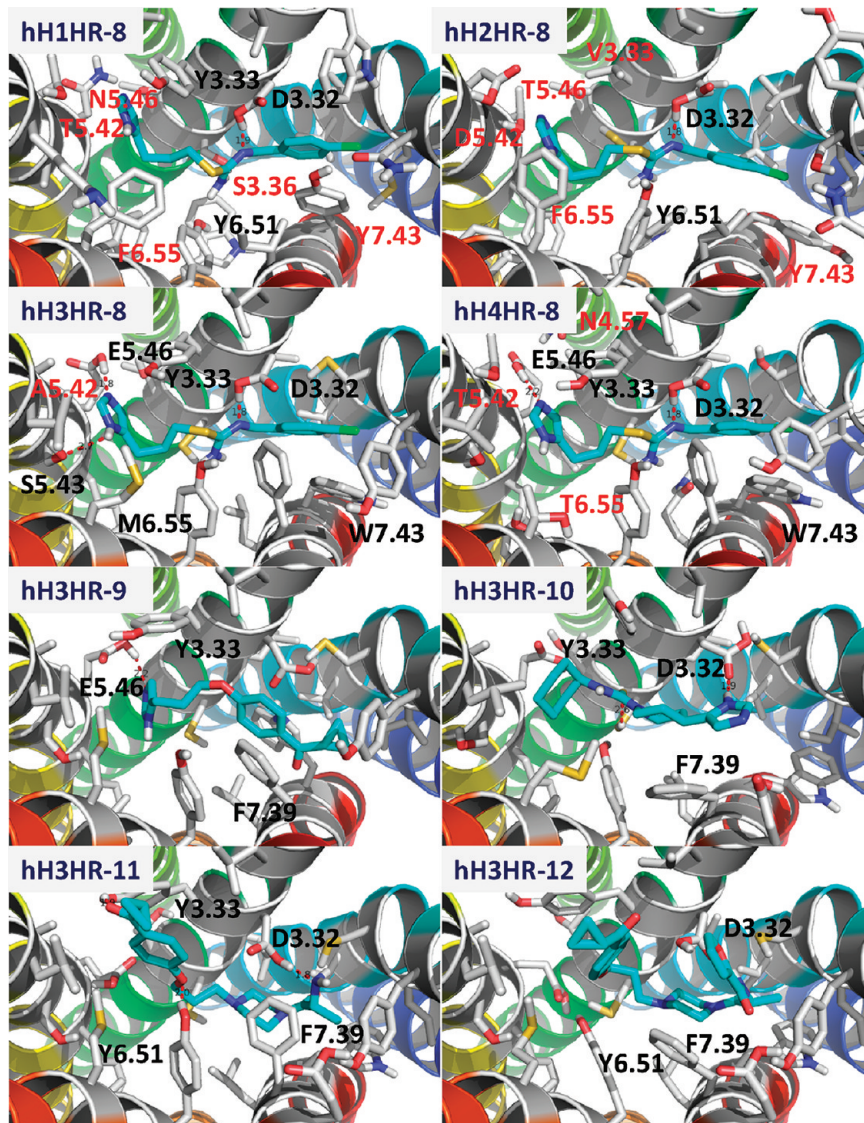


Figure 6. Predicted best models of the H_3 selective antagonist clobenpropit 8 bound to hH_1HR , hH_2HR , hH_3HR , hH_4HR and other antagonists, ciproxifan 9, thioperamide 10, A-304121 11, and A-317920 12 at hH_3HR . H-bonding is indicated by red dots, and subtype selective residues are shown in red.

describe the multiple functional forms of a receptor and would be unlikely to predict the important configurations of other GPCRs.

The GEnSeMBLE method applied in this paper was developed to enable exhaustive sampling of the conformational space to sample the variety of packings explored by receptors. We expect that this procedure dramatically increases the likelihood of predicting accurate structures for functionally distinct conformations of a GPCR and for predicting the structures of other more distant GPCRs. As additional GPCRs are crystallized to more fully cover both sequence space and function space (through G protein or β arrestin coupled pathways), such de novo prediction methods should increase in accuracy because of additional templates to initiate the process. Our results indicate that starting with a template for a crystal for one subtype of a GPCR, we can obtain accurate structures for the other subtypes. Also given a crystal structure of one GPCR, we can obtain accurate structures for other GPCRs that are within $\sim 30\%$ sequence identify for the TM regions.

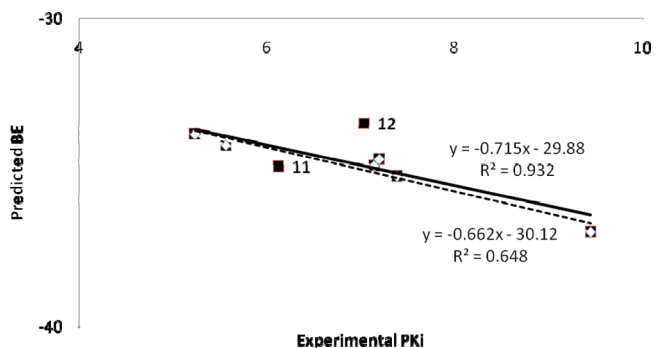


Figure 7. Predicted binding energies (kcal/mol) to the H_3 selective antagonist clobenpropit 8 bound to hH_1HR , hH_2HR , hH_3HR , hH_4HR and other antagonists, ciproxifan 9, thioperamide 10, A-304121 11, and A-317920 12 at hH_3HR listed in Table 5 compared with the experimental binding constants ($\text{p}K_i$). The dotted line shows the fit without two outliers, 11 and 12, which is much more flexible than the others.

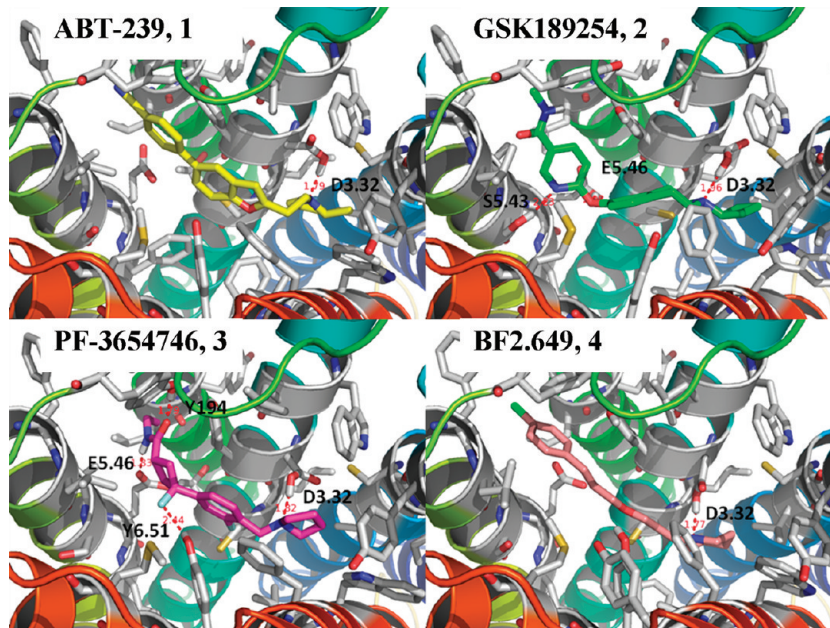


Figure 8. Predicted binding sites of structurally known hH₃HR in clinical study, ABT-239 **1**, GSK-189,254 **2**, and PF-3654746 **3**, and BF2.649 (tiprolisant) **4** at hH₃R. H-bonding is indicated by red dots.

■ CONCLUSIONS

We docked several H₃ selective ligands to all four subtypes to determine the critical components defining H₃ subtype selectivity with respect to the other three subtypes obtained. Our predictions of the best conformations of the histamine at H₁, H₂, H₃, and H₄ receptors subtypes lead to several conclusions: (1) The largest contribution to binding of the H₃ selective agonists (**5**, **6**, **7**) is E206^{5,46} in good agreement with the experimental mutational studies; (2) We find that the conserved E5.46/S5.43 in both of hH₃HR and hH₄HR are involved in H₃/ H₄ subtype selectivity through additional H-bonding with the terminal imidazole group in the monoalkyl-substituted imidazole-based derivatives but loss of these interactions in hH₁HR and hH₂HR. In addition, M378^{6,55} in hH₃HR is another subtype selective residue provides additional hydrophobic stabilization different from hH₄HR (the corresponding amino acid of T323^{6,55} in hH₄HR); (3) Our proposed pharmacophore model suggests that the residues important for selectivity to hH₃HR are: the basic proton interacting with D114^{3,32}, the spacer, the aromatic ring substituted with the hydrophilic or lipophilic groups interacting with lipophilic pockets in TMs 3–5–6, and the aliphatic ring located in TMs 2–3–7.

We expect our predicted 3D structures for all four HRs will help guide the rational design of novel H₃ subtype selective antagonists and agonists with reduced side effects. The excellent agreement with current experimental studies, particularly the understanding of H₃ subtype selectivity indicates that computationally derived structures of GPCRs can be sufficiently accurate to develop subtype selective drug to minimize side effects.

■ METHODS

We used the GENSeMBLE method² to predict the 3D structures for the various conformations needed to understand the function of GPCRs and help design new ligands. GENSeMBLE provides a very complete sampling (millions to quadrillions)

over possible rotations and tilts, leading to an ensemble of low-lying structures expected to include those conformations energetically accessible for binding of ligands. This replaces our earlier MembStruk method.³¹

We use the DarwinDock to predict the binding sites of ligands to the GPCRs. DarwinDock samples ~20 conformations for ~50 000 poses expanding the predicted binding sites, which we consider to be a very complete sampling. DarwinDock replaces our earlier HierDock⁶ and MSCDock³² methods, providing a much more complete sampling of possible poses. These earlier methods were validated by a series of applications to various GPCRs: human D₂ dopamine receptor (DR),³³ human β₂ adrenergic receptor,^{34,35} human M₁ muscarinic receptor,³⁶ human Chemokine (C–C) motif receptor 1 (CCR1),³⁷ mouse MrgC11 (mas related gene) for the molluscan peptide FMRFamide (FMRFa),^{38,39} human prostanoid DP receptor,⁴⁰ human Serotonin 2C,¹⁸ and human A_{2A} adenosine⁴¹ receptor.

GENSeMBLE⁴¹. The structure prediction methodology has been described previously⁴¹ so it will only be briefly summarized here:

- (1) **PredicTM:** This uses multiple sequence alignment to predict the TM regions for membrane protein.
- (2) **OptHelix/Homologize:** OptHelix generate helices with proper kinks (may be caused by Prolines) using molecular dynamics. However when closely related X-ray structures are available (as for the HRs), we find that homology helices often provide better helix shapes.
- (3) **BiHelix:** This algorithm samples all N⁷ packings of the 7 helices in a GPCR in which N rotations about each helix are combine. Here we consider N = 13, which leads to ~63 million conformations. BiHelix partitions the 7-helix interaction problem into 12 sets of BiHelix interactions, in which SCREAM¹⁷ is used to optimize the side chains for each combination.
- (4) **CombiHelix:** BiHelix energies for all 63 million packings are used to select the best 1000. Then we build the full

Table 6. RMSD Matrix between Predicted Histamine Receptors (top1 from BiHelix in Table 1) and the Recently Reported 3.1 Å Crystal Structure of the hH₁HR (PDB ID: 3RZE)¹¹

All TMs	hH1HR	hH2HR	hH3HR	hH4HR	3RZE
hH1HR	0.00	1.03	0.04	1.01	1.33
hH2HR	1.03	0.00	1.03	0.23	1.64
hH3HR	0.04	1.03	0.00	1.01	1.33
hH4HR	1.01	0.23	1.01	0.00	1.60
3RZE	1.33	1.64	1.33	1.60	0.00
TM1	hH1HR	hH2HR	hH3HR	hH4HR	3RZE
hH1HR	0.00	0.41	0.05	0.35	0.85
hH2HR	0.41	0.00	0.40	0.19	1.00
hH3HR	0.05	0.40	0.00	0.33	0.84
hH4HR	0.35	0.19	0.33	0.00	0.92
3RZE	0.85	1.00	0.84	0.92	0.00
TM2	hH1HR	hH2HR	hH3HR	hH4HR	3RZE
hH1HR	0.00	0.41	0.05	0.45	0.65
hH2HR	0.41	0.00	0.41	0.24	0.68
hH3HR	0.05	0.41	0.00	0.44	0.66
hH4HR	0.45	0.24	0.44	0.00	0.72
3RZE	0.65	0.68	0.66	0.72	0.00
TM3	hH1HR	hH2HR	hH3HR	hH4HR	3RZE
hH1HR	0.00	0.26	0.04	0.27	0.57
hH2HR	0.26	0.00	0.26	0.17	0.68
hH3HR	0.04	0.26	0.00	0.27	0.57
hH4HR	0.27	0.17	0.27	0.00	0.67
3RZE	0.57	0.68	0.57	0.67	0.00
TM4	hH1HR	hH2HR	hH3HR	hH4HR	3RZE
hH1HR	0.00	0.47	0.04	0.40	0.84
hH2HR	0.47	0.00	0.48	0.23	0.97
hH3HR	0.04	0.48	0.00	0.41	0.85
hH4HR	0.40	0.23	0.41	0.00	0.93
3RZE	0.84	0.97	0.85	0.93	0.00
TM5	hH1HR	hH2HR	hH3HR	hH4HR	3RZE
hH1HR	0.00	0.21	0.03	0.22	0.67
hH2HR	0.21	0.00	0.21	0.18	0.61
hH3HR	0.03	0.21	0.00	0.22	0.66
hH4HR	0.22	0.18	0.22	0.00	0.58
3RZE	0.67	0.61	0.66	0.58	0.00
TM6	hH1HR	hH2HR	hH3HR	hH4HR	3RZE
hH1HR	0.00	0.34	0.03	0.36	0.73
hH2HR	0.34	0.00	0.33	0.16	0.73
hH3HR	0.03	0.33	0.00	0.36	0.73
hH4HR	0.36	0.16	0.36	0.00	0.70
3RZE	0.73	0.73	0.73	0.70	0.00
TM7	hH1HR	hH2HR	hH3HR	hH4HR	3RZE
hH1HR	0.00	0.32	0.03	0.34	0.79
hH2HR	0.32	0.00	0.32	0.27	0.71
hH3HR	0.03	0.32	0.00	0.35	0.79
hH4HR	0.34	0.27	0.35	0.00	0.69
3RZE	0.79	0.71	0.79	0.69	0.00

helix bundle for each of these 1000 and optimize the side chains for each using SCREAM. From this 1000, we select an ensemble of ~ 10 lowest energy structures, each of which is used in docking of various ligands.

The Dreiding D3 force field (D3FF)⁴² was used throughout, wherever energies were evaluated.

Ligand Docking. DarwinDock was used to dock several ligands to each of the lowest 10 predicted structures of all 4 hHRs from BiHelix. The starting structure and charges of the ligands in Chart 1 were calculated using density functional theory (B3LYP with the 6-311G** basis set).

Starting from the X-ray structure of histamine, we rotated the torsion angles N—C_{al}—C_{al}—C_{ar} by 60° increments to generate 6 conformations. These were generated with the Maestro software and minimized with the D3FF. The final docked structure with the best binding *E* from all ligand conformations was selected.

Scanning the Receptor for Potential Binding Regions. Starting with the predicted structure, we predicted putative ligands binding regions as follows: We first alanized the entire protein (replacing the 6 hydrophobic residues, I, L, V, F, Y, and W with A) and scanned for potential binding regions with no assumption about the binding site. The entire molecular surface of the predicted structure was mapped with spheres representing the empty volume of the protein (currently using the Sphgen procedure in DOCK4.0 suite of programs). The entire set of protein spheres was partitioned into $\sim 30\text{--}50$ overlapping cubes of 10–14 Å sides. We then generated 1000 poses for each of these 30–50 regions. These results are compared to select the most promising two or three putative binding regions.

DarwinDock. For each ligand conformation, we used DarwinDock to generate iteratively $\sim 50\,000$ poses spanning the putative binding regions of the bulky residue-alanized protein. These poses are partitioned into ~ 1200 to ~ 200 family head Voronoi-like families based on RMSD, and then calculated the energies of the family heads and selected the top 10% ordered by total energy. Next we calculated the binding energy for all the family members of these top 10% family and selected the lowest energy 100 structures for further optimization. For each of these 100, we dealanize the protein side chains (using SCREAM) to find the optimum side chains for each of the best 100 poses. Then we neutralize the protein and the ligand by transferring protons appropriately within salt bridges and protonating or deprotonating exterior ligands, followed by further full geometry minimization.

DarwinDock has been validated for a number of X-ray cocrystals including 3 crystal structures of ligand/GPCR complexes: human β_2 -adrenergic receptor (0.4 Å RMSD),¹⁵ human AA_{2A}R (0.8 Å RMSD),⁴³ and turkey β_1 -adrenergic receptor (0.1 Å RMSD).¹⁶ This shows that DarwinDock can accurately identify ligand binding sites in proteins, which can then be used to optimize the ligands with desirable properties.

Neutralization for Scoring *E*. Quantum mechanics (QM) calculations show that for an effective dielectric constant below 8, the extra proton on a Lys or Arg transfers back to the negative carboxylate of an Asp or Glu. Thus we expect that buried salt bridges will have neutral residues. We find that use of these neutral residue charges for the protein and the ligand improves the accuracy for comparing different docked structures. Of course the final bond energy relative to ligand in the solvent and binding site exposed to solvent must be corrected by the effective pK_A of the ligand and of the exposed Lys, Arg, Glu, and Asp. For example, if the pK_A of a carboxylate is 4.5 and the solvent is taken to have a pH of 7.4, we must correct by 2.9×1.38 kcal/mol.

For external residues not involved in binding, we also find it is expected to neutralize the external residues exposed to solvent or membrane. Here the issue is that the force fields commonly used in molecular dynamic calculations involve fixed charges, usually

based on QM. In reality any net partial charges are shielded by the dielectric polarization of the surrounding protein and solvent, so that there is negligible effect beyond 10 Å. However with fixed charges, the electrostatic interaction energy between two point charges separated by 10 Å is 33 kcal/mol. The result is that small changes in geometries of charged ligands far from the binding site can lead to large differential binding energies, even 10–30 kcal/mol. We find that neutralizing these exposed residues removes the sensitivity to details of the distances of charged residues (and counterions) remote from the active site. This neutralization leads to differential binding energies that are dominated by the local cavity interactions and leads to much smaller solvation energies.¹⁸

■ ASSOCIATED CONTENT

Supporting Information. Sequence identities of four human HRs and X-ray structures, $t\beta_1$ AR, $h\beta_2$ AR, hAA_2 AR, and bovine rhodopsin (Table S1); overview of residue numbering for the TM regions in each of the four HRs based on homology to $t\beta_1$ AR and human β_2 adrenergic receptor (Table S2). This information is available free of charge via the Internet at <http://pubs.acs.org>.

■ AUTHOR INFORMATION

Corresponding Author

*E-mail: wag@wag.caltech.edu. Telephone: 1-626-395-2731

■ ACKNOWLEDGMENT

Funding for this project was provided by gifts to the Materials and Process Simulation Center (MSC) at California Institute of Technology, Pasadena, CA. P.F. thanks the Carlsberg Foundation, Lundbeck Foundation, and the Danish Council for Independent Research Technology and Production Sciences for financial support. In addition some funding was provided by NIH (R01NS071112 and 1R01NS073115).

■ REFERENCES

- (1) Lorenzi, S.; Mor, M.; Bordi, F.; Rivara, S.; Rivara, M.; Morini, G.; Bertoni, S.; Ballabeni, V.; Barocelli, E.; Plazzi, P. V. Validation of a histamine H3 receptor model through structure-activity relationships for classical H3 antagonists. *Bioorg. Med. Chem.* **2005**, *13*, 5647–5657.
- (2) Abrol, R.; Bray, J. K.; Goddard, W. A., III BiHelix: Towards de novo Structure Prediction of an Ensemble of G-Protein Coupled Receptor Conformations. *Proteins* **2011**, DOI: 10.1002/prot.23216.
- (3) Nissinen, M. J.; Karlstedt, K.; Castren, E.; Panula, P. Expression of histidine decarboxylase and cellular histamine-like immunoreactivity in rat embryogenesis. *J. Histochem. Cytochem.* **1995**, *43*, 1241–1252.
- (4) Hough, L. B. Genomics meets histamine receptors: New subtypes, new receptors. *Mol. Pharmacol.* **2001**, *59*, 415–419.
- (5) Berlin, M.; Boyce, C. W.; de Lera Ruiz, M. Histamine H3 Receptor as a Drug Discovery Target. *J. Med. Chem.* **2010**, *54*, 26–53.
- (6) Kiss, R.; Kiss, B.; Konczol, A.; Szalai, F.; Jelinek, I.; Laszlo, V.; Noszal, B.; Falus, A.; Keseru, G. M. Discovery of Novel Human Histamine H4 Receptor Ligands by Large-Scale Structure-Based Virtual Screening. *J. Med. Chem.* **2008**, *51*, 3145–3153.
- (7) Carballo, F. Efficiency of potent gastric acid inhibition. *Drugs* **2005**, *65*, 105–111.
- (8) Pettit, M. Treatment of gastroesophageal reflux disease. *Pharm. World Sci.* **2005**, *27*, 432–435.
- (9) Schneider, E. H.; Strasser, A.; Thurmond, R. L.; Seifert, R. Structural requirements for inverse agonism and neutral antagonism of indole-, benzimidazole-, and thienopyrrole-derived histamine H4 receptor ligands. *J. Pharmacol. Exp. Ther.* **2010**, *334*, 513–521.
- (10) Ligneau, X.; Morisset, S.; Tardivel-Lacome, J.; Gbahou, F.; Ganellin, C. R.; Stark, H.; Schunack, W.; Schwartz, J.-C.; Arrang, J.-M. Distinct Pharmacology of rat and human histamine H3 receptors: role of two amino acids in the third transmembrane domain. *Br. J. Pharmacol.* **2000**, *131*, 1247–1250.
- (11) Shimamura, T.; Shiroishi, M.; Weyand, S.; Tsujimoto, H.; Winter, G.; Katritch, V.; Abagyan, R.; Cherezov, V.; Liu, W.; Han, G. W.; Kobayashi, T.; Stevens, R. C.; Iwata, S. Structure of the human histamine H1 receptor complex with doxepin. *Nature* **2011**, *475*, 65–70.
- (12) Katoh, K.; Kuma, K.; Toh, H.; Miyata, T. MAFFT version 5: improvement in accuracy of multiple sequence alignment. *Nucleic Acid Res.* **2005**, *33*, 511–518.
- (13) Wimley, W. C.; Creamer, T. P.; White, S. H. Solvation energies of amino acid side chains and backbone in a family of host-guest pentapeptides. *Biochemistry* **1996**, *35*, 5109–5124.
- (14) Hessa, T. M.-B.; Bernsel, A.; Kim, H.; Sato, Y.; Lerch-Bader, M.; Nilsson, I.; White, S. H.; von Heijne, G. Molecular code for transmembrane-helix recognition by the Sec61 translocon. *Nature* **2007**, *450*, 1026–1030.
- (15) Cherezov, V.; Rosenbaum, D. M.; Hanson, M. A.; Rasmussen, S. G. F.; Thian, F. S.; Kobilka, T. S.; Choi, H.-J.; Kuhn, P.; Weis, W. I.; Kobilka, B. K.; Stevens, R. C. High-resolution crystal structure of an engineered human beta2-adrenergic G protein-coupled receptor. *Science* **2007**, *318*, 1258–1265.
- (16) Warne, T.; Serrano-Vega, M. J.; Baker, J. G.; Moukhametkhanov, R.; Edwards, P. C.; Henderson, R.; Leslie, A. G. W.; Tate, C. G.; Schertler, G. F. X. Structure of a β 1-adrenergic G-protein coupled receptor. *Nature* **2008**, *454*, 486–491.
- (17) Kam, V. W. T.; Goddard, W. A., III Flat-Bottom Strategy for Improved Accuracy in Protein Side-Chain Placements. *J. Chem. Theory Comput.* **2008**, *4*, 2160–2169.
- (18) Bray, J. K.; Goddard, W. A., III The structure of human serotonin 2c G-protein-coupled receptor bound to agonists and antagonists. *J. Mol. Graphics Modell.* **2008**, *27*, 66–81.
- (19) Venable, J. D.; Thurmond, R. L. Development and chemistry of histamine H4 receptor ligands as potential modulators of inflammatory and allergic diseases. *Anti-Inflammatory Anti-Allergy Agents Med. Chem.* **2006**, *5*, 307–322.
- (20) Stark, H.; Kathmann, M.; Schlicker, E.; Schunack, W.; Schlegel, B.; Sippl, W. Medicinal chemical and pharmacological aspects of imidazole-containing histamine H3 receptor antagonists. *Mini Rev. Med. Chem.* **2004**, *4*, 965–977.
- (21) Letavic, M. A. Recent medicinal chemistry of the histamine H3 receptor. *Prog. Med. Chem.* **2006**, *44*, 181–206.
- (22) Brioni, J. D.; Esbenshade, T. A.; Garrison, T. R.; Bitner, S. R.; Cowart, M. D. Discovery of Histamine H3 Antagonists for the Treatment of Cognitive Disorders and Alzheimer's Disease. *J. Pharmacol. Exp. Ther.* **2011**, *336*, 38–46.
- (23) Esbenshade, T. A.; Fox, G. B. K.; Miller, K. M.; Kang, T. R.; Denny, C. H.; Witte, L. I.; Yao, D. G.; Pan, B. B.; Wetter, L.; Marsh, J.; Bennani, K.; Cowart, Y. L.; Sullivan, M. D.; Hancock, J. P. A. A. Pharmacological properties of ABT-239 [4-(2-[{2(R)-2-Methyl-pyrrolidinyl}ethyl]-benzofuran-5-yl)benzonitrile]: I. Potent and selective histamine H3 receptor antagonist with drug-like properties. *J. Pharmacol. Exp. Ther.* **2005**, *313*, 165–175.
- (24) Medhurst, A. D.; Atkins, A. R.; Beresford, I. J.; Brackenborough, K.; Briggs, M. A.; Calver, A. R.; Cilia, J.; Cluderay, J. E.; Crook, B.; Davis, J. B.; Davis, R. K.; Davis, R. P.; Dawson, L. A.; Foley, A. G.; Gartlon, J.; Gonzalez, M. I.; Heslop, T.; Hirst, W. D.; Jennings, C.; Jones, D. N.; Lacroix, L. P.; Martyn, A.; Ociepka, S.; Ray, A.; Regan, C. M.; Roberts, J. C.; Schogger, J.; Southam, E.; Stean, T. O.; Trail, B. K.; Upton, N.; Wadsworth, G.; Wald, J. A.; White, T.; Withington, J.; Woolley, M. L.; Worby, A.; Wilson, D. M. GSK189254, a novel H3 receptor antagonist that binds to histamine H3 receptors in Alzheimer's disease brain and improves cognitive performance in preclinical models. *J. Pharmacol. Exp. Ther.* **2007**, *321*, 1032–1045.
- (25) Ligneau, X.; Perrin, D.; Landais, L.; Camelin, J. C.; Calmel, T. P.; I, B.-B.; Lecomte, J. M.; Parmentier, R.; Anacle, C.; Lin, J. S.; Bertaina-Anglade, V.; la Rochelle, C. D.; d'Aniello, F.; Rouleau, A.;

- Gbahou, F.; Arrang, J. M.; Ganellin, C. R.; Stark, H.; Schunack, W.; Schwartz, J. C. BF2.649 [1-[3-[3-(4-Chlorophenyl)propoxy]propyl]-piperidine, Hydrochloride], a Nonimidazole Inverse Agonist/Antagonist at the Human Histamine H3 Receptor: Preclinical Pharmacology. *J. Pharmacol. Exp. Ther.* **2007**, *320*, 365–375.
- (26) Uveges, A. J.; Kowal, D.; Zhang, Y.; Spangler, T. B.; Dunlop, J.; Semus, S.; Jones, P. G. The role of transmembrane Helix 5 in agonist binding to the human H3 receptor. *J. Pharmacol. Exp. Ther.* **2002**, *301*, 451–458.
- (27) Shin, N.; Coates, E.; Murgolo, N. J.; Morse, K. L.; Bayne, M.; Strader, C. D.; Monsma, F. J., Jr. Modular modeling and site-specific mutagenesis of the histamine-binding site of the histamine H4 receptor. *Mol. Pharmacol.* **2002**, *62*, 38–47.
- (28) Jongejan, A.; Lim, H. D.; Smits, R. A.; de Esch, I. J. P.; Haaksma, E.; Leurs, R. Delineation of agonist binding to the human histamine H4 receptor using mutational analysis, homology modeling, and ab initio calculations. *J. Chem. Inf. Model.* **2008**, *48*, 1455–1463.
- (29) Lim, H. D.; van Rijn, R. M.; Ling, P.; Bakker, R. A.; Thurmond, R. L.; Leurs, R. Evaluation of Histamine H1-H2-, and H3-Receptor Ligands at the Human Histamine H4 Receptor: Identification of 4-Methylhistamine as the First Potent and Selective H4 Receptor Agonist. *J. Pharmacol. Exp. Ther.* **2005**, *314*, 1310–1321.
- (30) Esbenshade, T. A.; Krueger, K. M.; Miller, T. R.; Kang, C. H.; Denny, L. I.; Witte, D. G.; Yao, B. B.; Fox, G. B.; Faghah, R.; Bennani, Y. L.; Williams, M.; Hancock, A. A. Two novel and selective nonimidazole histamine H3 receptor antagonists A-304121 and A-317920: I. In vitro pharmacological effects. *J. Pharmacol. Exp. Ther.* **2003**, *305*, 887–896.
- (31) Vaidehi, N.; Floriano, W. B.; Trabanino, R.; Hall, S. E.; Freddolino, P.; Choi, E. J.; Goddard, W. A., III Structure and Function of GPCRs. *Proc. Natl. Acad. Sci. U.S.A.* **2002**, *99*, 12622–12627.
- (32) Cho, A. E.; Wendel, J. A.; Vaidehi, N.; Kekenes-Huskey, P. M.; Floriano, W. B.; Maiti, P. K.; Goddard, W. A., III The MPSim-Dock Hierarchical Docking Algorithm: Application to the eight trypsin Inhibitor co-crystals. *J. Comput. Chem.* **2005**, *26*, 48–71.
- (33) Kalani, Y.; Vaidehi, N.; Hall, S. E.; Floriano, W. B.; Trabanino, R. J.; Freddolino, P. L.; Kam, V.; Goddard, W. A., III Three-dimensional structure of the human D2 dopamine receptor and the binding site and binding affinities for agonists and antagonists. *Proc. Natl. Acad. Sci. U.S.A.* **2004**, *101*, 3815–3820.
- (34) Freddolino, P. L.; Kalani, M. Y.; Vaidehi, N.; Floriano, W. B.; Trabanino, R. J.; Freddolino, P. L.; Kam, V.; Goddard, W. A., III Structure and function prediction for human b2-adrenergic receptor. *Proc. Natl. Acad. Sci. U.S.A.* **2004**, *101*, 2736–2741.
- (35) Spijker, P.; Vaidehi, N.; Freddolino, P. L.; Hilbers, P. A.; Goddard, W. A., III Dynamic behavior of fully solvated b2-adrenergic receptor, embedded in the membrane with bound agonist or antagonist. *Proc. Natl. Acad. Sci., U.S.A.* **2006**, *103*, 4882–4887.
- (36) Peng, J. Y.; Vaidehi, N.; Hall, S. E.; Goddard, W. A., III The Predicted 3D Structures of the Human M1Muscarinic Acetylcholine Receptor with Agonist or Antagonist Bound. *Chem. Med. Chem.* **2006**, *1*, 878–890.
- (37) Vaidehi, N.; Schlyer, S.; Trabanino, R. J.; Floriano, W. B.; R. A.; Sharma, S.; Kochanny, M.; Koovakat, S.; Dunning, L.; Liang, M.; Fox, J. M.; de Mendonca, F. L.; Pease, J. E.; Goddard, W. A., III; Horuk, R. Predictions of CCR1 Chemokine Receptor Structure and BX 471 Antagonist Binding Followed by Experimental Validation. *J. Biol. Chem.* **2006**, *281*, 27613–27620.
- (38) Heo, J.; Han, S.-K.; Vaidehi, N.; Wendel, J.; Kekenes-Huskey, P.; Goddard, W. A., III Prediction of the 3D Structure of FMRF-amide Neuropeptides Bound to the Mouse MrgC11 GPCR and Experimental Validation. *Chem. Bio. Chem.* **2007**, *8*, 1527–1539.
- (39) Heo, J.; Vaidehi, N.; Wendel, J.; Goddard, W. A., III Prediction of the 3-D structure of rat MrgA G protein-coupled receptor and identification of its binding site. *J. Mol. Graphics Modell.* **2007**, *26*, 800–812.
- (40) Li, Y.; Zhu, F.; Vaidehi, N.; Goddard, W. A., III; Sheinerman, F.; Reiling, S.; Morize, I.; Mu, L.; Harris, K.; Ardati, A.; Laoui, A. Prediction of the 3D structure and dynamics of human DP G-protein coupled receptor bound to an agonist and an antagonist. *J. Am. Chem. Soc.* **2007**, *129*, 10720–10731.
- (41) Goddard, W. A., III; Kim, S.-K.; Li, Y.; Trzaskowski, B.; Griffith, A. R.; Abrol, R. Predicted 3D structures for adenosine receptors bound to ligands: Comparison to the crystal structure. *J. Struct. Biol.* **2010**, *170*, 10–20.
- (42) Mayo, S. L.; Olafson, B. D.; Goddard, W. A., III DREIDING - a generic force field for molecular simulations. *J. Phys. Chem.* **1990**, *94*, 8897–8909.
- (43) Jaakola, V. P.; Griffith, M. T.; Hanson, M. A.; Cherezov, V.; Chien, E. Y.; Lane, J. R.; Ijzerman, A. P.; Stevens, R. C. The 2.6 angstrom crystal structure of a human A2A adenosine receptor bound to an antagonist. *Science* **2008**, *322*, 1211–1277.